


Dynamic modeling of barrier island response to hurricane storm surge under future sea level rise

Davina L. Passeri¹  · Matthew V. Bilskie^{2,3} ·
Nathaniel G. Plant⁴ · Joseph W. Long⁴ ·
Scott C. Hagen^{2,3}

Received: 4 December 2017 / Accepted: 26 June 2018

© This is a U.S. government work and its text is not subject to copyright protection in the United States; however, its text may be subject to foreign copyright protection 2018

Abstract Sea level rise (SLR) has the potential to exacerbate the impacts of extreme storm events on the coastal landscape. This study examines the coupled interactions of SLR on storm-driven hydrodynamics and barrier island morphology. A numerical model is used to simulate the hydrodynamic and morphodynamic impacts of two Gulf of Mexico hurricanes under present-day and future sea levels. SLR increased surge heights and caused overwash to occur at more locations and for longer durations. During surge recession, water level gradients resulted in seaward sediment transport. The duration of the seaward-directed water level gradients was altered under SLR; longer durations caused more seaward-directed cross-barrier transport and a larger net loss in the subaerial island volume due to increased sand deposition in the nearshore. Determining how SLR and the method of SLR implementation (static or dynamic) modulate storm-driven morphologic change is important for understanding and managing longer-term coastal evolution.

Key Points: SLR modulates the interaction between storm-driven hydrodynamics and morphologic evolution SLR increases dune overwash and alters seaward cross-barrier transport and nearshore deposition Static and dynamic implementations of SLR result in different interactions and impacts

Electronic supplementary material The online version of this article (<https://doi.org/10.1007/s10584-018-2245-8>) contains supplementary material, which is available to authorized users.

✉ Davina L. Passeri
dpasseri@usgs.gov

¹ U.S. Geological Survey St. Petersburg Coastal and Marine Science Center, 600 4th Street South, St. Petersburg, FL, USA

² Center for Coastal Resiliency, Louisiana State University, Baton Rouge, LA, USA

³ Department of Civil & Environmental Engineering/Center for Computation & Technology, Louisiana State University, Baton Rouge, LA, USA

⁴ U.S. Geological Survey St. Petersburg Coastal and Marine Science Center, St. Petersburg, FL, USA

1 Introduction

Tropical and extratropical storms reshape barrier island morphology with increasingly larger effects as oceanic water levels approach and exceed dune elevations. Impact regimes include swash (minor sand eroded on the beach), collision (erosion of the dune face with sand transported offshore), and overwash (overtopping of the dune crest with sand transported landward and deposited on the backside of the island) (Sallenger 2000; Stockdon et al. 2012; Stockdon et al. 2007). If water levels on both sides of the island exceed the dune crest, the island will become inundated, allowing water level gradients between the ocean and the bay to control flows and sediment transport (Long et al. 2014; Sallenger 2000; Stockdon et al. 2007). Depending on wind patterns, storm track and coastal geometry, water levels may slope from the bay to the ocean. This gradient drives flow and transport seaward, which can result in scour channels and sand deposition in the nearshore (Engelstad et al. 2017; Harter and Figlus 2017; Hoekstra et al. 2009; Sherwood et al. 2014).

Barrier islands depend on the accumulation of overwash deposition during individual storm events to persist and migrate landward (i.e., rollover) during periods of sea level rise (SLR) (Lorenzo-Trueba and Ashton 2014). In the future, SLR will cause a storm of a given magnitude to produce higher surge and more inundation; this will result in more frequent exceedances of morphologic thresholds and greater occurrences of morphologic change (Fitzgerald et al. 2008). Many studies have shown that storm surge heights under SLR increase nonlinearly (i.e., by more or less than the amount of SLR) (Atkinson et al. 2013; Bilskie et al. 2016a; Bilskie et al. 2014; Hagen and Bacopoulos 2012a; Mousavi et al. 2011; Smith et al. 2010; Yin et al. 2017). However, the role of sea level in storm-driven hydrodynamic-morphodynamic interactions has not been explored. This study examines the morphodynamic response of a barrier island (Dauphin Island, Alabama) to storm surge under SLR. A large-domain hydrodynamic model was used to simulate hurricanes Ivan (2004) and Katrina (2005) under present-day conditions and projections of future SLR. Model output was used to force XBeach (Roelvink et al. 2009), a process-based model that simulates storm-driven morphology. Results illustrate the triple-coupled interactions and feedbacks between sea level, storms, and morphology, and improve the understanding of longer-term barrier island evolution in the context of storm events.

2 Study domain

Dauphin Island is a segmented low-lying barrier island located off the Alabama coast (Fig. 1). The undeveloped western end is low in elevation with dune heights generally less than 1.5 m, NAVD88. The developed eastern end has higher dunes on the order of 3 m. The island is positioned between the Gulf of Mexico and the Mississippi Sound. Northeast of the island, Mobile Bay connects to the Mississippi Sound through Pass aux Herons, a shallow shoaled inlet that separates mainland marshes from Dauphin Island. Landward of the island, the Mississippi Sound is shallow, with bathymetric depths ranging from 2 to 4 m.

During storm events, the geometric and topographic characteristics of offshore bathymetry and barrier islands in the Gulf of Mexico drive complex hydrodynamic processes that can cause substantial storm surge and significant morphologic change (Bilskie et al. 2016b).

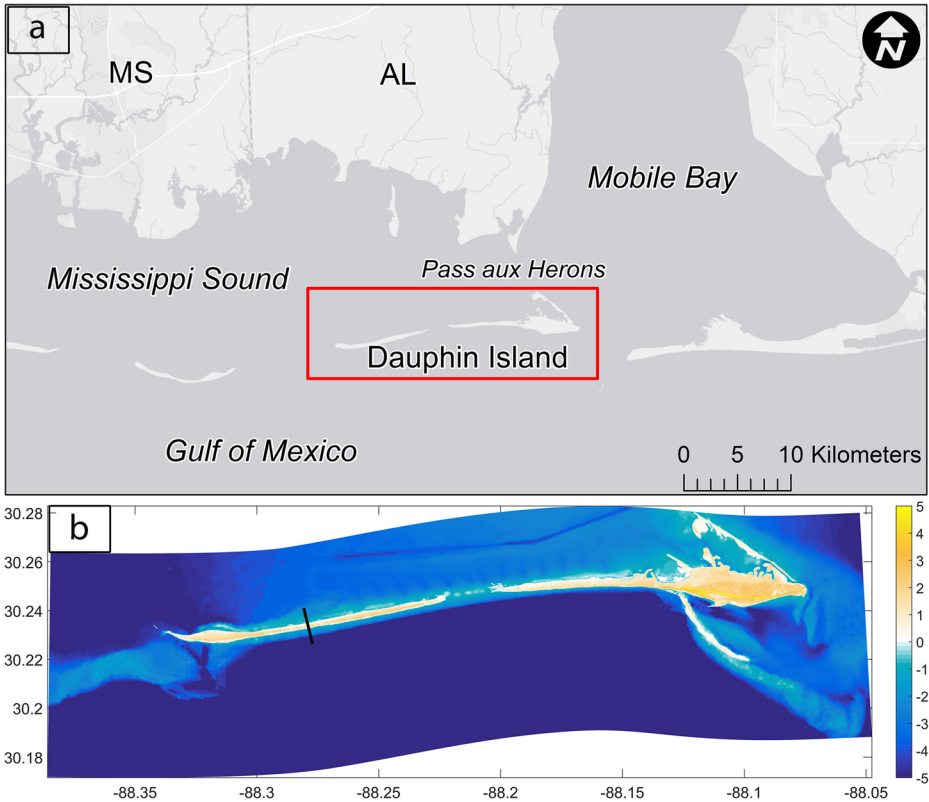


Fig. 1 **a** Study area, **b** XBeach model domain, and present-day elevations (m, NAVD88). Black line indicates location of representative cross-shore transect analyzed in Fig. 2

Historically, the morphology of Dauphin Island has changed dramatically as a result of storm-driven overwash and breaching. In 2004, Hurricane Ivan caused extensive overwash and fragmented the middle of Dauphin Island. A year later, Hurricane Katrina caused a breach approximately 2000 m wide in the middle of the island (Morton 2008).

3 Dynamic modeling approach

To observe the morphodynamic response of Dauphin Island to the combined impacts of storm surge, waves, and SLR, a dynamic modeling approach was implemented. Sediment transport and bed level change were simulated using XBeach, a two-dimensional depth-averaged model that solves the nonlinear shallow water equations and incorporates time-varying wave action balance and roller energy balance (Roelvink et al. 2009). Sediment transport is calculated with a depth-averaged advection-diffusion equation (Galappatti and Vreugdenhil 1985), in which an equilibrium sediment concentration determines increases or decreases in sediment concentration in the water column (Soulsby 1997). The model simulates morphologic change from the swash, collision, overwash, and inundation storm-impact regimes (Sallenger 2000). A 2DH description of infragravity waves (i.e., frequency less than 0.04 hz (Herbers et al. 1995)) allows water levels to vary on the shoreface. Mass seaward flux from waves and rollers is directed

offshore in the form of depth-averaged return flow, which allows for continuous erosion of the dune face with offshore deposition. Sediment is transported from the dry dune face to the wet swash through an avalanching algorithm that is triggered by infragravity swash run-up paired with a specified critical wet slope. Wave-group forcing in combination with a momentum-conserving wetting and drying algorithm results in a landward flux of momentum, which lowers dune elevations and transports sediment onshore in overwash fans. Breaches are resolved from sediment transport induced by dynamic channel flow and avalanche-triggered bank erosion (Roelvink et al. 2009). Previous studies have shown XBeach is capable of simulating storm-driven dune erosion, overwash, inundation, breaching, and seaward sand transport with high skill (Harter and Figlus 2017; Lindemer et al. 2010; McCall et al. 2010; Passeri et al. 2018; Roelvink et al. 2009; Sherwood et al. 2014).

The XBeach grid encompasses Dauphin Island and has a constant alongshore resolution of 25 m and a varying cross-shore resolution down to 3 m on the subaerial island (Passeri et al. 2018). Hindcast analyses showed that this model was able to capture storm-driven morphologic change associated with Ivan and Katrina; see Passeri et al. (2018) for details. For this study, topographic and bathymetric elevations were derived from a 3-m resolution, post-Katrina digital elevation model (DEM) of the Mobile Bay region (Danielson et al. 2013) (Fig. 1). As described in Passeri et al. (2018), spatially varying bed friction coefficients were parametrized using 2011 land use/land cover (LULC) data obtained from the Coastal Change Analysis Program (C-CAP). Other model parameters used to calibrate short-wave hydrodynamics; flow, sediment transport, and bed update were set to the default values as specified in McCall et al. (2010).

The XBeach model was forced with time-series water levels and wave spectra extracted from *NGOM3* (Bilskie et al. 2016b), a 5.5-million node ADCIRC+SWAN model that computes water surface elevations, depth-integrated velocities, and wave radiation stresses. *NGOM3* was validated for Ivan and Katrina and used to establish a physics-based modeling framework to simulate hurricane storm surge under future SLR scenarios (Bilskie et al. 2016a, b). For this study, *NGOM3* was forced with astronomic tides and meteorological wind and pressure fields for Ivan and Katrina. Each storm was simulated under present-day conditions and projections of low and intermediate-low SLR (0.20 and 0.50 m, respectively), obtained from Parris et al. (2012). These scenarios were selected to observe the morphologic sensitivity of a low-elevation barrier island to plausible increases in sea level over the next century. To incorporate SLR, *NGOM3*'s initial mean sea level was offset by the amount of SLR (i.e., the eustatic method (Bilskie et al. 2016a)); this dynamic approach ensures that nonlinearities in the governing equations are captured, which permits more accurate assessments than the static or "bathtub" approach, in which present-day water levels are simply elevated by the amount of SLR (Hagen and Bacopoulos 2012a). Following the model setup of Passeri et al. (2018), hourly water levels for Ivan were extracted from *NGOM3* at the middle of the seaward and landward XBeach grid boundaries to account for cross-shore water level gradients at the middle of the domain. Hourly significant wave heights, mean wave directions, and peak wave periods were extracted at the middle of the seaward boundary and used to generate a time-series of JONSWAP spectra that was applied uniformly along the offshore boundary. For Katrina, hourly water levels were extracted from *NGOM3* at the four corners of the XBeach grid to account for alongshore gradients in surge northwest of the island. Wave conditions were applied to the seaward boundary similar to the Ivan simulation.

4 Results

4.1 Hurricane Ivan

Hurricane Ivan made landfall as a Category 3 storm at 06:50 UTC 16 September near Gulf Shores, AL (Stewart 2004). Hindcast simulations from *NGOM3* indicate that as Ivan approached, easterly winds caused a vertical rise in water levels in western Mobile Bay. After landfall, westerly winds caused surge to build up on the east side of the Mississippi Sound behind Dauphin Island (Bilskie et al. 2016b). The bathymetry of Pass aux Herons formed a “pocket” behind the island, which resulted in a seaward-directed (i.e., towards the Gulf of Mexico) water level gradient as surge recessed. In the low and intermediate-low scenarios, peak surge increased nonlinearly from the present-day scenario especially at the landward boundary; see Online Resource 1 for complete time-series water level and wave boundary conditions, as well as peak surge elevations.

Instantaneous water levels and bed levels across the domain were output hourly from XBeach. From this output, the inundated area (calculated as the difference between the initial dry area of the island, defined from the 0, 0.20, and 0.50 m contours for each scenario, and the area not wetted during the simulation), the net loss in subaerial island volume (calculated as the difference between the initial volume of the subaerial island and the volume of the post-storm subaerial island), the percentage of dunes that experienced overwash (i.e., if the water level was higher than the dune crest and the dune crest stayed in the same position or moved landward), and the average hours of overwash are summarized in Table 1; post-storm bed levels and changes in pre- and post-storm bed levels are illustrated in Figs. 1 and 2 of Online Resource 2, respectively. Inundation increased with SLR across the island from 87.2% in the present-day scenario to 97.2% under low SLR and 98.7% under intermediate-low SLR. Higher water levels caused more widespread overwash (55.6% of dunes in the present-day scenario, 76.7% under low SLR, and 78.8% under intermediate-low SLR) for longer durations (an average of 9.7 h in the present-day scenario, 24.1 h under low SLR, and 27.8 h under intermediate-low SLR). Despite increased inundation and more overwash, the net loss in the subaerial island volume was nonlinear under higher sea levels; low SLR resulted in

Table 1 Area of island inundated, initial subaerial island volume, net loss in the subaerial island volume, percentage of dunes that experience overwash, and average hours each dune experiences overwash for Ivan and Katrina scenarios

Scenario	Area of island inundated	Initial subaerial island volume (millions of m ³)	Net loss in subaerial island volume (millions of m ³)	% dunes overwash	Hours of overwash
Ivan					
Present day	87.2%	18.7	0.95 (5.1%)	55.6%	9.7
Low	97.2%	16.0	1.29 (8.0%)	76.7%	24.2
Int. low	98.7%	12.2	0.63 (5.2%)	78.8%	27.8
Static low	88.1%	16.0	0.49 (3.0%)	65.0%	12.3
Static int. low	94.5%	12.2	0.36 (3.0%)	68.6%	14.2
Katrina					
Present day	99.5%	18.7	2.24 (12.0%)	80.1%	17.3
Low	99.6%	16.0	1.65 (10.3%)	81.2%	28.8
Int. low	99.7%	12.2	1.00 (8.1%)	82.1%	31.1

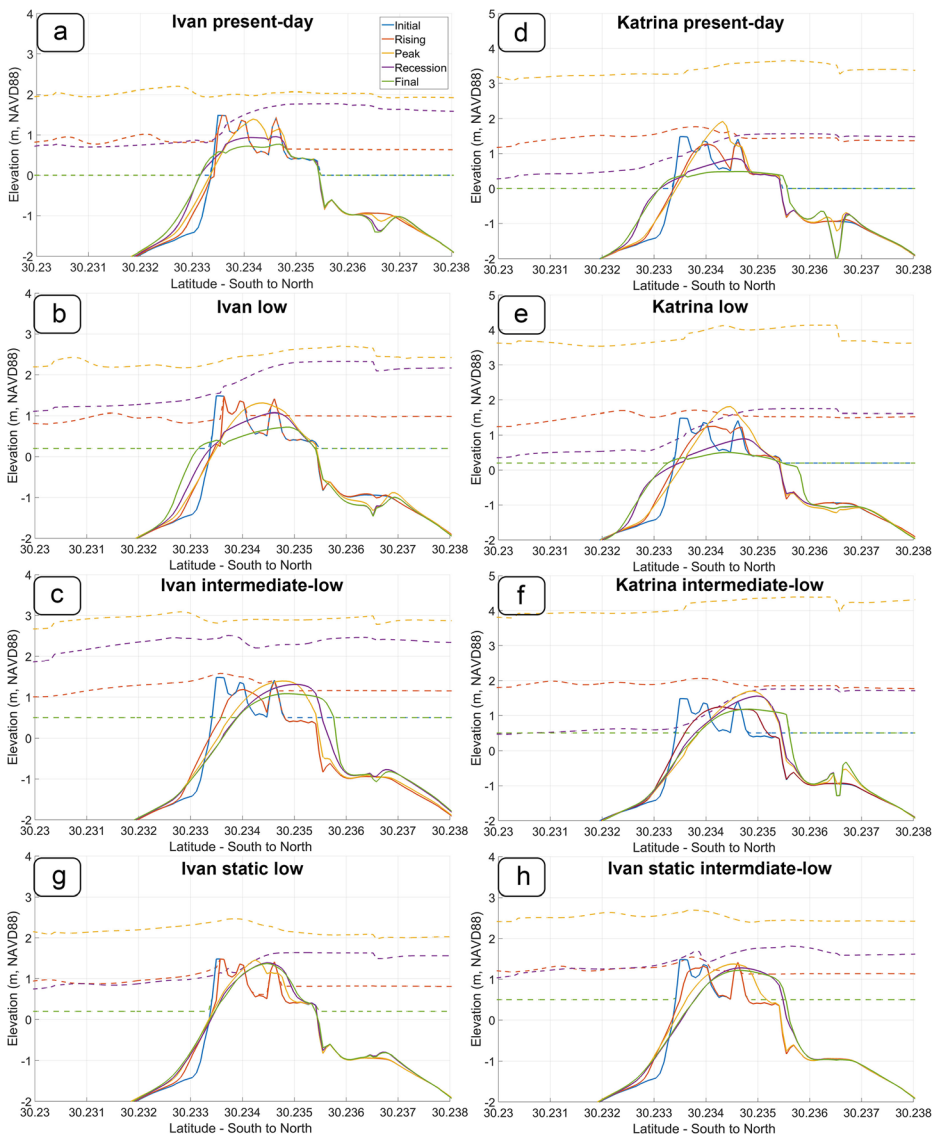


Fig. 2 Initial, rising limb, peak, recession, and final water levels (dotted lines) and bed levels (solid lines) plotted at the transect (x -axis is latitude in decimal degrees): **a** Ivan present day, **b** Ivan low, **c** Ivan intermediate low, **d** Katrina present day, **e** Katrina low, **f** Katrina intermediate low, **g** Ivan static low, and **h** Ivan static intermediate low

the largest net loss (8.0%) compared to 5.1% in the present-day scenario and 5.2% under intermediate-low SLR.

The interactions and feedbacks between hydrodynamic and morphodynamic processes vary through the duration of a storm. To explore this, a representative cross-shore transect on the western end of the island was selected (see Fig. 1 for location). Water level and bed level elevations were extracted at the beginning of the simulation (12:00 UTC 13 Sept), during the rising limb of the storm (13:00 UTC 15 Sept), during peak surge (4:00 UTC 16 Sept), during

surge recession (8:00 UTC 16 Sept), and at the end of the storm (12:00 UTC 17 Sept) (Fig. 2). In the present-day and low SLR scenarios, the dune was in collision during the rising limb and sand was eroded from the dune face and deposited seaward of the Gulf shoreline, herein referred to as the nearshore. In the intermediate-low SLR scenario, water levels during the rising limb exceeded the dune crest and caused overwash. As water levels reached a maximum, the dune crest was inundated in all three scenarios causing overwash; after the storm made landfall, water level gradients were directed seaward. The post-storm bed level elevations for the present-day and low SLR scenarios show seaward cross-barrier transport with sand deposition in the nearshore. There was less of a water level gradient in the intermediate-low scenario and the post-storm bed level elevation indicates that the dune continued to experience overwash with landward sand deposition exceeding the position of the pre-storm backbarrier shoreline (i.e., the island was rolling over). The developed eastern end of the island exhibited similar morphologic behavior as the western end, except higher dune elevations reduced the magnitude and duration of overwash and seaward transport.

Since seaward-directed water level gradients drive seaward cross-barrier transport, understanding the behavior of these gradients through the duration of the storm is as important as understanding the impact of surge heights. The magnitude of the gradient at the transect, measured from 110 m landward and seaward of the 0 m contour, was calculated for each hour of the simulation (see Online Resource 4 for further discussion on the water level gradient calculation). Figure 3 shows the time-series of gradient magnitudes, the subaerial transect profile area (defined from the pre-storm shoreline) and the hours when overwash and seaward transport occurred. In the present-day scenario, overwash began 36 h into the simulation, at which point the subaerial profile area began to increase as a result of sand being transported from the nearshore to the backbarrier. One hour after peak surge, seaward-directed water level gradients increased to 0.010 and induced seaward transport, which lasted for 4 h as the gradient reached a maximum magnitude of 0.017. During this time, the subaerial profile area decreased due to deposition in the nearshore. Towards the end of the storm, the island experienced a small resurgence wave that briefly increased the gradient magnitude to 0.013 and caused seaward transport for two more hours (a total of 6 h). In the low SLR scenario, overwash began 32 h into the simulation and the subaerial profile area increased until peak water levels. Seaward transport began 2 h after peak water levels when the water level gradient magnitude reached 0.010 and lasted for 4 h with a maximum magnitude of 0.018. During this time, the subaerial profile area decreased due to sand deposition in the nearshore. Seaward transport stopped until the resurgence wave, which increased the water level gradient to 0.014 and caused seaward transport for five more hours (a total of 9 h). In the intermediate-low SLR scenario, overwash began 29 h into the simulation, again increasing the subaerial profile area until peak surge. After peak surge, the water level gradient magnitude was lower than the present-day and low SLR scenarios (maximum of 0.010) and seaward transport only occurred for 1 h.

4.2 Hurricane Katrina

Hurricane Katrina made landfall as a Category 3 storm at 11:00 UTC 29 August near Buras, LA (Knabb et al. 2005). Hindcast simulations from *NGOM3* illustrate that southeasterly winds elevated water levels in the Mississippi Sound as Katrina approached. After landfall, water levels remained higher in the Mississippi Sound, which caused a seaward-directed water level

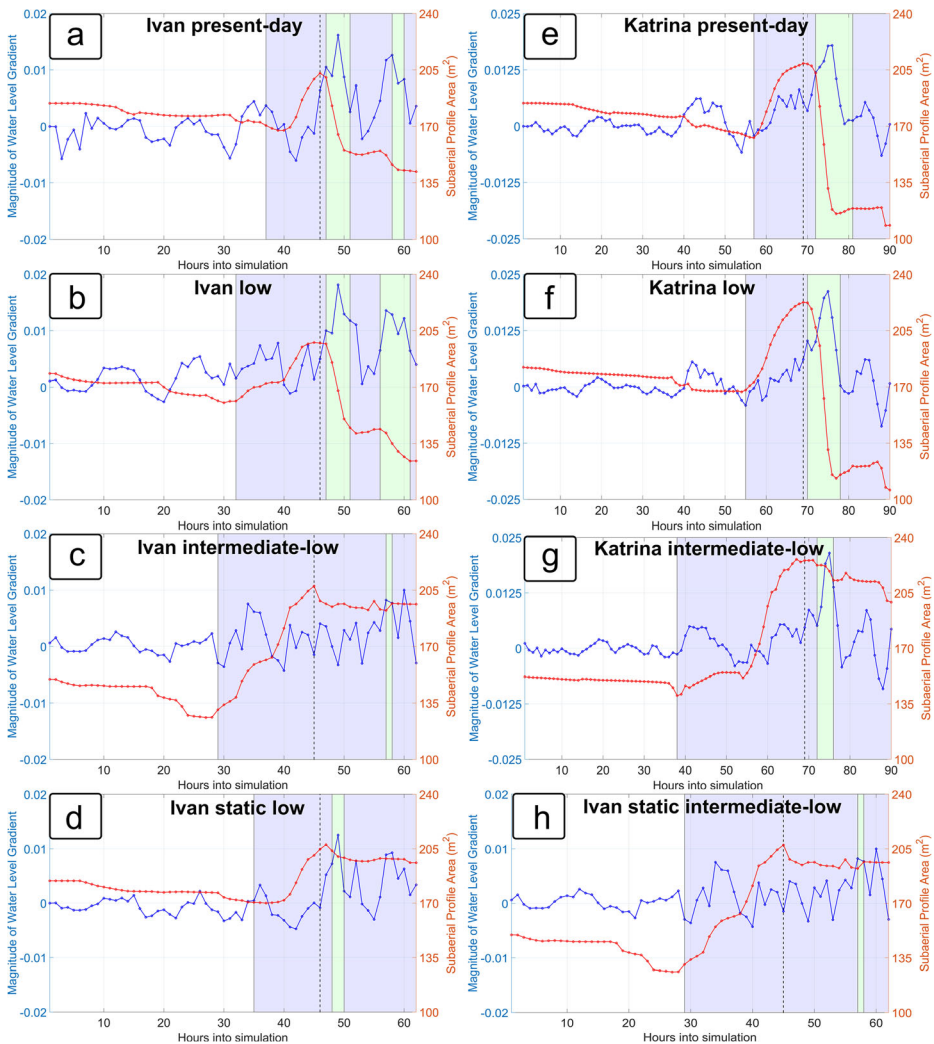


Fig. 3 Magnitude of water level gradients (blue line) and subaerial profile area (red line) at the transect shown in Fig. 2: **a** Ivan present day, **b** Ivan low, **c** Ivan intermediate low, **d** Ivan static low, **e** Katrina present day, **f** Katrina low, **g** Katrina intermediate low, and **h** Ivan static intermediate low. Positive gradients indicate higher water levels landward of the island (i.e., seaward sloping). Purple-shaded regions indicate times when overflow occurred, green shaded regions indicate times when seaward-directed transport occurred, dotted black vertical line indicates time of peak surge. Latitudes of where the water level gradient was calculated across the transect are 30.232 and 30.327, as shown in Fig. 2

gradient across Dauphin Island (Bilskie et al. 2016b). Low and intermediate-low SLR increased peak surge almost linearly (i.e., equal to the amount of SLR) at the northeast corner of the XBeach grid and slightly less than the amount of SLR at the northwest, southwest, and southeast corners; see Online Resource 1 for complete time-series water level and wave boundary conditions, as well as peak surge elevations.

Inundation and erosion metrics are summarized in Table 1 and post-storm bed levels are illustrated in Online Resource 2. In the present-day scenario, the island was almost completely inundated (99.5%), resulting in 80.1% of the dunes in overflow for an average of 17.3 h and a

net loss of 12.0% in the subaerial island volume. Under low SLR, the percentage of dunes in overwash was similar to the present-day scenario (81.2%), but the average hours of overwash increased to 28.8; the net loss in the subaerial island volume decreased to 10.3%. This trend continued with the intermediate-low SLR scenario, in which the percentage of dunes in overwash increased to 82.1%, the average hours of overwash increased to 31.1, and the net loss in the subaerial island volume decreased to 8.1%.

Figure 2 shows water level and bed level elevations at the representative transect on the western end of the island at the beginning of the simulation (0:00 UTC 27 Aug), during the rising limb of the storm (4:00 UTC 29 Aug), during peak surge (14:00 UTC 29 Aug), during recession (20:00 UTC 29 Aug), and at the end of the storm (12:00 UTC 30 Aug). In the present-day and low SLR scenarios, water levels overtopped the dune crest during the rising limb of the storm, resulting in overwash. In the intermediate-low SLR scenario, high tide water levels before the storm (8:00 UTC 28 Aug) inundated the dune and caused overwash; this resulted in further landward sand deposition during the rising limb than in the present-day and low SLR scenarios. As water levels reached a maximum, there was overwash in all three scenarios. During recession, seaward-directed water level gradients resulted in seaward transport; post-storm bed level elevations show nearshore sand deposition in the present-day and low SLR scenarios but minimal nearshore deposition in the intermediate-low SLR scenario.

Similar to the Ivan scenarios, seaward-directed water level gradients induced cross-barrier transport which altered the net loss in the subaerial island volume. Figure 3 illustrates that under higher sea levels, overwash began earlier (2 and 8 h earlier than present-day for low and intermediate-low SLR, respectively); this increased the subaerial profile area due to increased sand transport from the nearshore to the backbarrier. The hours of seaward transport decreased with increased SLR. In the present day scenario, seaward transport started when the magnitude of the gradient reached 0.0125 and continued for 9 h with a maximum magnitude of 0.019. In the low SLR scenario, seaward transport occurred for 8 h after peak surge with a maximum gradient magnitude of 0.021. In the intermediate-low SLR scenario, seaward transport occurred after peak surge for 4 h with a maximum gradient magnitude of 0.020. In all scenarios, seaward transport decreased the subaerial profile area due to sand deposition in the nearshore; longer durations of seaward transport resulted in more transport and a larger net loss in the subaerial island volume.

5 Discussion

The results of this study advance the findings of previous studies that have focused on the interactions of sea levels and storms, by including possible morphologic outcomes of these interactions. The relationship between increased storm-induced water levels due to SLR and the net loss in the subaerial island volume was nonlinear for the Ivan scenarios. There was a larger net loss in volume in the low SLR scenario than in the present-day and intermediate-low SLR scenarios as a result of longer durations of seaward-directed water level gradients, which caused more seaward transport and deposition in the nearshore. Changes in the water level gradient resulted from the nonlinear response of the hydrodynamics due to the interactions of increased water levels and topography/bathymetry. When SLR is a significant portion of the total water column depth, peak surge heights are amplified; this occurs for smaller increments of SLR, less intense storms, areas with shallow bathymetry/topography or in “pockets” that are surrounded by topographic features on two or three sides (Atkinson et al. 2013; Bilskie et al.

2016a; Bilskie et al. 2014; Hagen and Bacopoulos 2012b; Smith et al. 2010). For Ivan, maximum water level elevations in the Mississippi Sound were amplified more for low SLR than intermediate-low SLR (Fig. 1, Online Resource 3) due to shallow bathymetry and the geometry of Pass aux Herons which created a pocket between the mainland and Dauphin Island. This amplification increased the magnitude and duration of the water level gradient during recession. In the intermediate-low SLR scenario, the pocket collapsed due to increased overtopping of Dauphin Island and widening of Pass aux Herons as higher water levels spread across the mainland marshes, which allowed more flow to/from Mobile Bay. Maximum water level elevations seaward and landward of the island were almost equal, which reduced the water level gradient during recession. The surge response to SLR was amplified for Ivan rather than Katrina because Ivan was a weaker storm that produced lower surge heights (Online Resource 3). For Katrina, maximum water level elevations in the low and intermediate-low SLR scenarios were increased by less than the amount of SLR due to higher water levels and onshore winds that caused surge to propagate further inland as the storm approached, thereby reducing surge in the Mississippi Sound (Fig. 1, Online Resource 3). During recession, the duration of the water level gradients was reduced as surge inundated new areas. These results further the understanding of how SLR can alter storm surge hydrodynamics not only in terms of peak surge, but also water level gradients during surge recession.

Previous studies have shown that seaward-directed water level gradients during inundation can be as important as onshore-directed waves in driving cross-barrier sediment transport (e.g., Harter and Figlus (2017), Passeri et al. (2018), and Sherwood et al. (2014)); this study adds to the examples through a comparison of multiple storms under multiple scenarios. Seaward-directed water level gradients were generated as a result of the storm characteristics of Ivan and Katrina and the geometry of the study area. After the storms made landfall, offshore waves and water levels started to subside but water levels remained high in the Mississippi Sound, which resulted in seaward-directed flows and transport. An increase in the offshore water levels and wave heights would reduce the seaward-directed water level gradient and wave-driven transport (overwash) would occur; this behavior was seen in the Ivan present-day scenario during the resurgence wave after landfall (Fig. 3; Online Resource 4).

Without a dynamic modeling approach, nonlinearities in the hydrodynamics would not have been captured and the simulated post-storm morphology would differ. To demonstrate this, two additional XBeach simulations were performed for Ivan using static water level boundary conditions for low and intermediate-low SLR. In these simulations, the amount of SLR was added to the present-day time-series water level boundary conditions (i.e., the static or “bathtub” approach). Table 1 shows that the static low SLR scenario resulted in less inundation (88.1%), less net loss in subaerial island volume (3.8%), a lower percentage of dunes in overwash spatially (65.0%), and less average hours of overwash (12.3) compared to the dynamic simulation. At the transect (Fig. 2), the dune experienced overwash as water levels reached a peak. During recession, landward water levels were lower than in the dynamic simulation, which reduced the water level gradient magnitude (maximum of 0.013) and limited seaward transport to 2 h (Fig. 3); overall, post-storm elevations were higher than the dynamic scenario and less sand was lost to the nearshore. The static intermediate-low SLR scenario also resulted in less inundated area (94.5%), less net loss in subaerial island volume (3.0%), a lower percentage of dunes in overwash spatially (68.6%) and less average hours of overwash (14.2) compared to the dynamic scenario (Table 1). At the transect, post-storm elevations were higher than in the dynamic simulation due to an under-prediction in the elevation of peak and recession water levels (Fig. 2); seaward transport only occurred for 1 h (Fig. 3). When

considering long-term interactions, even small variations in individual storm impacts have the potential to lead to large differences in expected morphologic evolution.

Understanding the evolution of barrier islands is critical for protecting coastal communities and mitigating future hazards such as storms and SLR. Changes in storm-driven overwash and nearshore deposition have implications for the future of barrier islands. Storm-driven nearshore deposition can aid in beach recovery or can be removed from the local barrier island sand budget via alongshore transport (Sherwood et al. 2014). Over longer periods, barrier islands depend on the accumulation of overwash deposition during storm events to persist and migrate landward during periods of SLR (Lorenzo-Trueba and Ashton 2014). The future of barrier islands will depend on the cumulative impacts of SLR, multiple storms, recovery, and restoration efforts. Although not considered in this study, the intensity of North Atlantic tropical cyclones may increase under warmer climates (Hartmann et al. 2013; Knutson et al. 2010; Villarni and Vecchi 2013), resulting in higher storm-induced wave heights and exacerbated erosion. Even without changes in storm intensity, rising sea levels will increase the frequency of strong waves and the magnitude of flow velocities during storm events, exposing barrier islands to higher wave-induced energy (Rovere et al. 2017). Also, long-term changes in elevation as the island adapts to increased sea levels were not considered. Although the interactions of sea levels, storms and morphology may differ for other locations or storm events, this three-way interaction needs to be considered (with both a static and dynamic approach) in studies modeling storm-driven barrier island morphology. This type of assessment will allow coastal managers to make more informed decisions when assessing the risk of future hazards or mitigation strategies (e.g., nourishment or dune rebuilding).

6 Conclusions

XBeach simulations of Ivan and Katrina at Dauphin Island, AL under present-day, low (0.20 m) and intermediate-low (0.5 m) SLR showed that higher sea levels resulted in increased inundation and more overwash spatially and for longer durations. Both storms produced seaward-directed water level gradients during recession, which caused seaward cross-barrier transport with deposition in the nearshore. Under SLR, changes in seaward-directed water level gradients were more nonlinear for Ivan than Katrina due to relative storm strength. For Ivan, low SLR amplified surge landward of the island, which increased the duration of seaward-directed water level gradients during recession and caused more seaward transport and a larger net loss in the subaerial island volume than in the present-day scenario. Intermediate-low SLR allowed more surge to flow to/from the Mississippi Sound, which reduced the water level gradient during recession and limited the duration of seaward transport and deposition in the nearshore. Implementing SLR with a dynamic approach resulted in more inundation, overwash, and erosion due to amplified surge heights and longer durations of seaward-directed water level gradients. For Katrina, higher SLR increased the magnitude of seaward-directed water level gradients during recession but decreased the duration due to additional surge propagation inland; this reduced seaward transport and the net loss in the subaerial island volume. The findings of this study advance the knowledge of how SLR alters storm surge hydrodynamics and illustrate potential impacts to morphology. Studies examining event-driven and long-term coastal evolution should consider the dynamic triple-coupled interactions and feedbacks between sea level, storms, and morphology.

Acknowledgments The model inputs and outputs for this study can be found in Passeri, D.L., Bilskie, M.V., Plant, N.G., Long, J.W., Hagen, S.C., 2018, Dauphin Island Storms and Sea Level Rise Assessment: XBeach Model Inputs and Results: U.S. Geological Survey data release, <https://doi.org/10.5066/F7N87930>. The authors would like to thank Soupy Dalyander at USGS and the anonymous reviewers for their constructive comments. Any use of trade, firm, or product names is for descriptive purposes only and does not imply endorsement by the U.S. Government.

Funding information This effort was funded in part under awards NA10NOS4780146 and NA16NOS4780208 from the National Oceanic and Atmospheric Administration (NOAA) Center for Sponsored Coastal Ocean Research (CSCOR).

References

- Atkinson JH, Smith JM, Bender C (2013) Sea-level rise effects on storm surge and nearshore waves on the Texas coast: influence of landscape and storm characteristics. *J Waterw Port Coast Ocean Eng* 139:98–117. [https://doi.org/10.1061/\(ASCE\)WW.1943-5460.0000187](https://doi.org/10.1061/(ASCE)WW.1943-5460.0000187)
- Bilskie MV, Hagen SC, Medeiros SC, Passeri DL (2014) Dynamics of sea level rise and coastal flooding on a changing landscape. *Geophys Res Lett* 41:927–234. <https://doi.org/10.1002/2013GL058759>
- Bilskie MV, Hagen SC, Alizad K, Medeiros SC, Passeri DL, Needham H, Cox A (2016a) Dynamic simulation and numerical analysis of hurricane storm surge under sea level rise with geomorphologic changes along the northern Gulf of Mexico. *Earth's Future* 4:177–193. <https://doi.org/10.1002/2015EF000347>
- Bilskie MV, Hagen SC, Medeiros SC, Cox AT, Salisbury M, Coggin D (2016b) Data and numerical analysis of astronomic tides, wind-waves, and hurricane storm surge along the northern Gulf of Mexico. *J Geophys Res Oceans* 121:3625–3658. <https://doi.org/10.1002/2015JC011400>
- Danielson JJ, Brock JC, Howard DM, Gesch DB, Bonisteel-Cormier JM, Travers LJ (2013) Topobathymetric model of Mobile Bay, Alabama. U.S. Geological Survey Data Series 769
- Engelstad A, Ruessink BG, Wesselman D, Hoekstra P, Oost A, van der Vegt M (2017) Observations of waves and currents during barrier island inundation. *J Geophys Res Oceans* 122:3152–3169. <https://doi.org/10.1002/2016JC012545>
- Fitzgerald DM, Fenster MS, Argow BA, Buynevich IV (2008) Coastal impacts due to sea-level rise. *Annu Rev Earth Plane Sci* 36:601–647. <https://doi.org/10.1146/annurev.earth.35.031306.140139>
- Galappatti G, Vreugdenhil CB (1985) A depth-integrated model for suspended sediment transport. *J Hydraul Res* 23:359–377. <https://doi.org/10.1080/00221688509499345>
- Hagen SC, Bacopoulos P (2012a) Coastal flooding in Florida's Big Bend Region with application to sea level rise based on synthetic storms analysis. *Terr Atmos Ocean Sci* 23:481–500. [https://doi.org/10.3319/TAO.2012.04.17.01\(WMH\)](https://doi.org/10.3319/TAO.2012.04.17.01(WMH))
- Hagen SC, Bacopoulos P (2012b) Synthetic storms contributing to coastal flooding in Florida's Big Bend Region with application to sea level rise. *Terr Atmos Ocean Sci* 23:481–500
- Harter C, Figlus J (2017) Numerical modeling of the morphodynamic response of a low-lying barrier island beach and foredune system inundating during Hurricane Ike using XBeach and CSHORE. *Coast Eng* 120: 64–74. <https://doi.org/10.1016/j.coastaleng.2016.11.005>
- Hartmann DL et al. (2013) Observations: atmosphere and surface. *Climate change 2013: The Physical Science Basis. Contribution of Working Group I to the Fifth Assessment Report of the Intergovernmental Panel on Climate Change*. Cambridge, UK
- Herbers THC, Elgar S, Guza RT (1995) Generation and propagation of infragravity waves. *J Geophys Res* 100: 24863–24872
- Hoekstra P, ten Haaf M, Buijs P, Oost A, Klein Breteler K, van der Giessen K, van der Vegt M (2009) Washover development on mixed-energy, mesotidal barrier island systems. In: Mizuguchi M, Sato S (eds) *Coastal dynamics*, vol. 83. World Scientific, Singapore, pp 25–32
- Knabb RD, Rhome JR, Brown DP (2005) Hurricane Katrina. National Oceanic and Atmospheric Administration National Weather Service Tropical Prediction Center, Miami
- Knutson TR et al (2010) Tropical cyclones and climate changes. *Nat Geosci* 3:157–163
- Lindemer CA, Plant NG, Puleo JA, Thompson DM, Wamsley TV (2010) Numerical simulation of a low-lying barrier island's morphologic response to Hurricane Katrina. *Coast Eng* 57:985–995. <https://doi.org/10.1016/j.coastaleng.2010.06.004>

- Long JW, de Bakker ATM, Plant NG (2014) Scaling coastal dune elevation changes across storm-impact regimes. *Geophys Res Lett* 41:1–8. <https://doi.org/10.1002/2014GL059616>
- Lorenzo-Trueba J, Ashton AD (2014) Rollover, drowning and discontinuous retreat: distinct modes of barrier response to sea-level rise arising from a simple morphodynamic model. *J Geophys Res Earth Surf* 119:779–801. <https://doi.org/10.1002/2013JF002941>
- McCall RT, Van Thiel de Vries J, Plant NG, Van Dongeren A, Thompson DM, Reniers A (2010) Two-dimensional time dependent hurricane overwash and erosion modeling at Santa Rosa Island. *Coast Eng* 57:668–683. <https://doi.org/10.1016/j.coastaleng.2010.02.006>
- Morton RA (2008) Historical changes in the Mississippi-Alabama Barrier-Island chain and the roles of extreme storms, sea level, and human activities. *J Coast Res* 24:1587–1600
- Mousavi M, Irish JL, Frey AE, Olivera F, Edge BL (2011) Global warming and hurricanes: the potential impact of hurricane intensification and sea level rise on coastal flooding. *Clim Chang* 104:575–597. <https://doi.org/10.1007/s10583-009-9790-0>
- Parris A et al (2012) Global sea level rise scenarios for the United States National Climate Assessment. NOAA Tech Memo OAR CPO-1, Silver Spring, p 37
- Passeri DL, Long JW, Plant NG, Bilskie MV, Hagen SC (2018) The influence of bed friction variability due to land cover on storm-driven barrier island morphodynamics. *Coast Eng* 132:82–94. <https://doi.org/10.1016/j.coastaleng.2017.11.005>
- Roelvink JA, Reniers A, van Dongeren A, van Thiel de Vries J, McCall R, Lescinski J (2009) Modeling storm impacts on beaches, dunes and barrier islands. *Coastal Eng* 56:1133–1152. <https://doi.org/10.1016/j.coastaleng.2009.08.006>
- Rovere A et al (2017) Giant boulders and last interglacial storm intensity in the North Atlantic. *PNAS* 114:12144–12149. <https://doi.org/10.1073/pnas.1712433114>
- Sallenger AHJ (2000) Storm impact scale for barrier islands. *J Coast Res* 16:890–895
- Sherwood CR, Long JW, Dickhudt PJ, Dalyander PS, Thompson DM, Plant NG (2014) Inundation of a barrier island (Chandeleur Islands, Louisiana, USA) during a hurricane: observed water-level gradients and modeled seaward and transport. *J Geophys Res Earth Surf* 119:1498–1515. <https://doi.org/10.1002/2013JF003069>
- Smith JM, Cialone MA, Wamsley TV, McAlpin TO (2010) Potential impact of sea level rise on coastal surges in southeast Louisiana. *Ocean Eng* 37:37–47. <https://doi.org/10.1016/j.oceaneng.2009.07.008>
- Soulsby RL (1997) Dynamics of marine sands: a manual for practical applications. Thomas Telford Publications, London, p 249
- Stewart SR (2004) Hurricane Ivan. National Oceanic and Atmospheric Administration, National Weather Service Tropical Prediction Center, Miami
- Stockdon HF, Sallenger AH, Holman R, Howd P (2007) A simple model for the spatially-variable coastal response to hurricanes. *Mar Geol* 238:1–20. <https://doi.org/10.1016/j.margeo.2006.11.004>
- Stockdon HF, Doran KJ, Thompson DM, Sopkin KL, Plant NG, Sallenger AH (2012) National assessment of hurricane-induced coastal erosion hazards: Gulf of Mexico. U.S. Geological Survey Open-File Report 2012–1084
- Villami G, Vecchi GA (2013) Projected increases in North Atlantic tropical cyclone intensity from CMIP5 models. *J Clim* 26:3231–3240
- Yin K, Xu S, Huang W, Xie Y (2017) Effects of sea level rise and typhoon intensity on storm surge and waves in Pearl River Estuary. *Ocean Eng* 136:80–93. <https://doi.org/10.1016/j.oceaneng.2017.03.016>